Assessment of variability in continental low stratiform clouds based on observations of radar reflectivity

Zena N. Kogan, David B. Mechem, and Yefim L. Kogan
Cooperative Institute for Mesoscale Meteorological Studies, University of Oklahoma, Norman, Oklahoma, USA

Received 29 April 2005; accepted 28 June 2005; published 22 September 2005.

[1] The variability of overcast low stratiform clouds observed over the ARM Climate Research Facility Southern Great Plains (ACRF SGP) site is analyzed, and an approach to characterizing subgrid variability based on assumed statistical distributions is evaluated. The analysis is based on a vast (>1000 hours) radar reflectivity database collected by the Millimeter-Wave Cloud Radar at ACRF SGP site. The radar data are classified into two low cloud categories and stratified by scale and the presence of precipitation. Cloud variability is analyzed by studying statistical distributions for the first two moments of the probability distribution functions (PDF) of radar reflectivity. Results indicate that variability for a broadly defined low-altitude stratiform cloud type exhibits on average 40% greater standard deviation than canonical boundary layer clouds topped by an inversion. Cloud variability also dramatically depends on microphysical processes (as manifested in radar reflectivity) and increases by 2–5 times within a typical reflectivity range. Finally, variability is a strong function of scale and almost doubles in the 20–100 min temporal scale range. Formulations of subgrid variability, based on PDFs of reflectivity, are evaluated for the two cloud types and two scales of 10 and 30 km, taken to be representative of mesoscale and NWP model grid sizes. The results show that for these cloud types and scales the PDF of reflectivity can be reasonably well approximated by a truncated Gaussian function, specified by mean and standard deviation with the latter parameterized as a linear function of the mean.

Citation: Kogan, Z. N., D. B. Mechem, and Y. L. Kogan (2005), Assessment of variability in continental low stratiform clouds based on observations of radar reflectivity, *J. Geophys. Res.*, *110*, D18205, doi:10.1029/2005JD006158.

1. Introduction

[2] Low layer clouds play a significant role in the Earth's radiative budget and, because of their high albedo, may globally decrease the net radiative forcing by 15 W m^{-2} [*Hartman et al.*, 1992]. These clouds are also closely tied to planetary boundary layer processes; therefore an understanding of their response to changes in forcing, entrainment, and the effects of drizzle is important in reducing the uncertainty of cloud radiative forcing. While marine low-layer clouds have been the focus of major field projects and extensive studies, in comparison continental low-layer clouds have historically been overlooked [*Del Genio et al.*, 1996].

[3] An important element of cloud characterization is a better understanding of cloud system variability, which it is hoped will lead to improved parameterizations of subgrid-scale cloud structure in numerical models. Neglecting variability can lead to substantial biases in radiative quantities [e.g., *Cahalan et al.*, 1994] and microphysical process rates, which can be highly nonlinear [e.g., *Rotstayn*, 2000; *Pincus and Klein*, 2000; *Larson et al.*, 2001a; *Wood et al.*, 2002; Y. L. Kogan, unpublished data, 1998]. These biases arise in cloudy grid volumes when microphysical or thermodynamic quantities are simply calculated from predicted grid point variables, an operation that assumes the quantity is homogeneous inside the grid volume. Unbiased process rates or radiative quantities can be calculated, provided the distribution function of relevant quantities is known. These distributions are typically specified as probability distribution functions (PDFs), with the parameters describing the PDF predicted or determined either from observational or model data. Because of the fundamental role PDFs play in characterizing variability, various theoretical aspects of PDF characterization have been examined in the number of recent studies [see, e.g., *Larson et al.*, 2001b; *Price*, 2001; *Larson et al.*, 2002; *Price and Wood*, 2002]; however, observational investigations of cloud system PDFs are relatively few.

[4] A class of cloud parameterization schemes usually referred to as cloud ''statistical schemes'' attempts to account for subgrid variability in clouds. These schemes describe cloud subgrid variability in each grid box by using a distribution function of an assumed analytical form and then determining its parameters. The approach follows the ideas of *Sommeria and Deardorff* [1977] and *Mellor* [1977] and was further developed in more recent studies [see, e.g., *Golaz et al.*, 2002; *Tompkins*, 2002; *Klein et al.*, 2005]. The most difficult part of this method lies in determining the parameters (moments) that dictate the PDFs. Model pre-

0148-0227/05/2005JD006158

dicted quantities are usually defined as grid volume averages and thus define the first PDF moment. A closure for the higher-order moments based on resolved model quantities can proceed from assumptions, theory, high-resolution numerical simulations, or observational data [*Tompkins*, 2002].

[5] In the present paper we explore the variability of low-layer clouds based on the radar reflectivity database collected by the Atmospheric Radiation Measurement Program (ARM) [*Ackerman and Stokes*, 2003]. Since January of 1997, ARM has operated continuously a Millimeter-Wave Cloud Radar (MMCR), located at the ARM Climate Research Facility (ACRF) Southern Great Plains site (SGP). Exploring variability of radar reflectivity has several important applications. First, information about radar reflectivity variability can be compared with synthesized reflectivities from numerical models to evaluate the performance of model cloud parameterizations or model performance in general. Second, our investigation of reflectivity variability uses a methodological approach that can be applied to a variety of scales for other variables as well. For example, the variability of quantities retrieved from reflectivity such as liquid water content and precipitation flux can be explored. We also note that, although current numerical models do not predict radar reflectivity, future cloud physics schemes may predict full moments of the drop size distribution function [see, e.g., *Belotchitski*, 2002] and thus would be able to apply directly PDFs of reflectivity in addition to other, more conventional quantities related to moments of the drop size distribution function, such as concentration, effective cross section, LWC, and precipitation flux.

[6] In the characterization of cloud variability we place special emphasis on cloud type and scale. For this purpose, we first analyze databases for two separate low cloud categories and then assess variability characteristics at fixed 10-km and 30-km scales. These scales may be taken as in the realm of characteristic grid sizes for mesoscale and numerical weather prediction (NWP) models. In addition, we attempt to represent reflectivity by known analytical functions, for example Gaussian or Gamma types. These analytical approximations have been tested in many previous studies [e.g., *Larson et al.*, 2001b], and this study will explore the advantages and limitations of analytical PDF approximations to the ARM SGP radar reflectivity data set.

[7] The paper is organized as following. Section 2 describes the data and presents climatological statistics of cloud system characteristics, such as duration and frequency of occurrence. Section 3 describes statistics of cloud variability in terms of PDFs and their first and second moments. In Section 4 we discuss the character of reflectivity variability at 10 and 30 km spatial scales and test how well analytic approximations represent the observed PDFs for evaluating precipitation flux biases and process rates in general. A summary and conclusions are presented in section 5.

2. Description of Data and Methodology

2.1. Conditional Sampling Technique

[8] Our analysis is based on approximately 1000 hours of radar reflectivity for low stratiform clouds observed over the Southern Great Plains ARM Climate Research Facility (ACRF) during two winter seasons (December–February 1997–1998 and January–March 2001) and March 2000 (the month of the ARM Cloud Intensive Operational Period). The ARM vertically pointing, 35 GHz (K_a band), Millimeter-Wave Cloud Radar (MMCR) supplies radar reflectivity data [*Moran et al.*, 1998; *Clothiaux et al.*, 2000]. The MMCR cycles through four modes of operation and an ARM Value Added Product (VAP) distills the data from these four modes into a "best estimate" of radar reflectivity. These data are supplied at ten second intervals and every 45 m in the vertical, which corresponds to the range gate spacing for radar operation modes 1 and 4.

[9] Backscattering hydrometeors in cloudy layers are assumed to be predominantly liquid phase. This assumption is reasonable given the shallow, low-level clouds. *Curry et al.* [2000] found that appreciable ice is unlikely to be present until cloud temperatures reach between −5 and −12°C, depending on the maximum droplet size. Temperatures for clouds in our data set are usually above this temperature range. Each element in the database represents a cloudy period corresponding to a time series $Z_i(t)$ of radar reflectivity (expressed as dBZ) measured in the middle portion of the cloud – which in nonprecipitating clouds corresponds approximately to the level of mean cloud liquid water content. Cloudy periods are included in the database only if continuously sampled by the radar for more than 500 s. This time threshold contains fifty, 10 s radar samplings and filters out shorter cloud segments that do not provide statistically robust estimates of the moments of radar reflectivity series. Cases with vertically overlapping clouds are also included in the analysis, except for identifiable periods in the radar imagery when precipitation from higher cloud layers contaminates the lower layer. In the latter case, the two layers merge and appear as one on the radar screen.

2.1.1. Discriminating by Cloud Type

[10] *Norris and Klein* [2000] used surface observations and NCEP–NCAR (National Centers for Environmental Prediction–National Center for Atmospheric Research) reanalysis data to stratify marine boundary layer cloud types as a function of synoptic regime. While no equivalent study exists for continental boundary layer clouds, a significant fraction of the cloud systems in our database bear striking resemblance to classical stratocumulus-topped boundary layers observed over the subtropical oceans. This type of winter season cloud system over the ACRF typically occurs under a strong inversion and is accompanied by large-scale subsidence divergence.

[11] In addition to the canonical boundary layer cloud type, a more general low cloud category exists, typically deeper and generally associated with strong synoptic forcing such as fronts or short-wave troughs. It is reasonable to expect that the different nature of the dynamical forcing between these two low cloud types might lead to different variability characteristics. For this reason, it seems natural to stratify the reflectivity data according to these two cloud system types. We identify these cloud categories subjectively, on the basis of cloud top height. The first category is boundary layer stratocumuli (BL) which are characterized by cloud tops below 1.5 km. The typical depth of clouds in the BL category is several hundred meters. The second

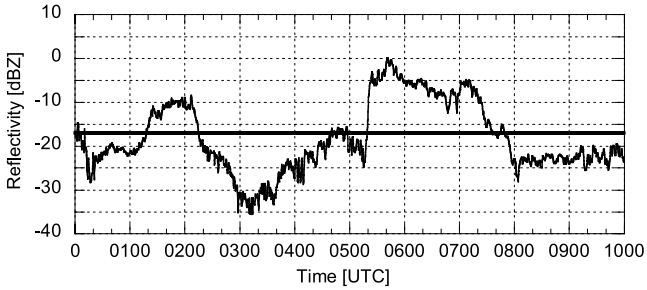

Figure 1. Reflectivity time series for BL cloud observed on 14 January 1998 from 0000 to 1000 UTC over the ACRF SGP site. Nonprecipitating segments are 0000–0122, 0215–0524, and 0750–1000 UTC. Precipitating segments are 0122–0215 and 0524–0750 UTC. The thick horizontal line corresponds to the −17 dBZ precipitation threshold.

category, low-altitude stratiform clouds (LA), is characterized by cloud top greater than 1.5 km; the typical depth of clouds in the LA category is one to three km. Comparing this classification with soundings shows that the cloud tops in the BL category are nearly always accompanied by a well defined temperature inversion. As we show in the following sections, the characterization of cloud system variability in terms of PDF moments for the two categories is more statistically robust than that for the full, original data set.

2.1.2. Discriminating by Drizzle

[12] Precipitation, in this case mostly in the form of drizzle, is a major component of the water budget whose presence significantly affects boundary layer thermodynamics, energetics, and dynamics [*Stevens et al.*, 1998]. Although the influence of drizzle on larger scales is poorly understood, we should expect variability characteristics to depend strongly on whether or not precipitation is present. The converse may also be true: clouds with greater variability caused by various mesoscale forcing mechanisms may experience a wider range of vertical motions and, as a result, an enhanced precipitation development. For this reason, we further stratified cloud segments into precipitating and nonprecipitating categories using a radar reflectivity threshold of −17 dBZ. This threshold follows from observational data which indicate that radar reflectivity values lower than −17 dBZ are usually associated with nonprecipitating cloud layers. The −17 dBZ threshold also tends to be well correlated with the presence of droplets greater than 50 μm in diameter, which we term drizzle. (The most common type of precipitation from low stratus is drizzle, so we will use terms precipitation and drizzle interchangeably.) A segment is categorized as precipitating (nonprecipitating) when 95% of the reflectivity samples within the segment are greater (less) than the −17 dBZ threshold. An example of how the data are partitioned into precipitating and nonprecipitating categories is demonstrated in Figure 1. In this case the 10 h cloudy period is stratified into three nonprecipitating and two precipitating segments. Since the time series are extracted from the middle of the cloud, the presence of drizzle applies within the cloud and does not necessarily indicate (nor does it preclude) drizzle falling anywhere in the subcloud layer. The fidelity of using a reflectivity threshold for discriminating between precipitating and nonprecipitating continental clouds is discussed in detail in Appendix A.

2.1.3. Discriminating by Scale

[13] Previous studies [e.g., *Oreopoulos and Davies*, 1998; *Liu et al.*, 2002; *Wood et al.*, 2002; *Li et al.*, 2005] have demonstrated significant scale dependence in cloud system variability. The obvious consequence of this dependence is that any parameterization of subgrid variability will be sensitive to scale, as determined by either the grid size in a finite difference scheme or the truncation characteristics in a spectral formulation. To study the scale dependence of low-level clouds and to what degree it depends on cloud type and precipitation (and the responsible microphysical processes), we resample all cloudy segments into subsegments of length 10, 15, 20, …, 180 minutes. Variability parameters are then calculated for each subsegment. Applying the "frozen turbulence" hypothesis the temporal scales can be transformed into spatial scales. We focus on two horizontal scales in particular, representative of a mesoscale (10 km) and NWP (30 km) grid sizes. The assumption of frozen turbulence introduces an error roughly proportional to the length of the analyzed scale. *Kim et al.* [2005] studied continental stratiform low-level clouds over the SGP and evaluated the temporal change in the mean value of optical thickness over the period of an hour ranged from 35–60% of the spatial standard deviation. For a fixed scale of 10 km (which translates to 16 min, assuming an advective speed of 10 m s^{-1}) we estimate the temporal variability in the mean to be 9–15% of the spatial variability. In other words, at this scale the variability arising from nonstationarity is only a small contribution to the total variability, indicating that the frozen turbulence assumption is reasonable. Nonstationarity may, however, be more significant for spatial scales of the order or larger than 30 km, and distinguishing between inherent mesoscale variability and temporal variation may be difficult using single-point measurements.

2.1.4. Notation

[14] The following notations are used henceforth. "BL" denotes the boundary layer cloud category, while "LA" denotes more general low-altitude clouds. Precipitating and nonprecipitating clouds add suffixes of "p" and "np." Subscripts of 10 and 30 denote subsegment sizes of 10 km and 30 km, respectively. Thus, from the full database come four sets of cloud system categories: BLnp, BLp, LAnp, and LAp. Corresponding sets for 10 and 30 km segments are $BLnp_{10}$, BLp_{10}, $LAnp_{10}$, and LAp_{10} and $BLnp_{30}$, BLp_{30}, $LAnp_{30}$, and LAp_{30}. Each of these sets has a corresponding ensemble of radar reflectivity time series $\{Z_i(t)\}$, and for each i segment in a particular set we calculated its $PDF_i(Z)$, mean reflectivity $\overline{Z}_i$ and standard deviation σ_i. Here, bars denote averages over segments.

2.2. Frequency of Occurrence and Duration

[15] Segment length and the frequency of precipitating and nonprecipitating segments provide a fundamental measure of macroscale variability. These statistics give a notion of "patchiness" and are closely tied to cloud system geometry. Table 1 shows that a total of more than 775 hours of overcast BL clouds were observed over 482 segments of variable length (temporal duration). The duration for 75% of

Table 1. Statistics on Number and Duration of Segments for Boundary Layer (BL) and Low-Altitude Stratiform Clouds (LA)

		Cloud Segment Duration, hours				
Cloud Type	Number of Segments	Total	Mean	Standard Deviation	Median	75th Percentile
BLnp	324	538.6 (69%)	1.7	1.9	0.97	2.2
BLp	158	236.8 (31%)	1.5	2.1	0.69	1.7
LAnp	112	77.6 (30%)	0.69	1.0	0.34	0.85
LAp	114	178.2 (70%)	1.56	2.0	0.69	2.1

the segments is less than 2.2 h, although a few segments have extraordinarily long durations of 11.2 h for BLnp and 17.2 h for BLp cloud segments. The average durations of nonprecipitating and precipitating BL segments are similar. However, because there are twice as many nonprecipitating segments as precipitating, they strongly dominate the duration statistics, and as a result, the ratio of nonprecipitating to precipitating durations over all observed BL clouds is 7:3. Half of the BLp clouds are lightly drizzling ($Z < -14$ dBZ); thus about 85% of all observed BL clouds are only lightly drizzling or not precipitating at all. Although the mean durations for BLp and BLnp categories are comparable, the BLnp category exhibits a greater number of long duration segments relative to BLp cloud systems. This makes sense, given the understanding that precipitation can enhance PBL cloud system variability (patchiness) by leading to thinning of the cloud layer and eventually a broken cloud field [*Stevens et al.*, 1998].

[16] A total of more than 255 hours of the low-altitude category (LA) were observed over 226 segments. LA clouds are less common than BL cloud systems, and LA cloud frequency of occurrence is about half that of the BL category. Table 1 shows that, in contrast to BL clouds, the LA clouds are predominantly precipitating with the ratio of duration between nonprecipitating and precipitating segments being 3:7. It is remarkable that the number of LAnp and LAp segments is almost the same, but the LAp segments are on average 2.3 times longer than their LAnp counterparts. This difference likely arises from the stronger contribution of the mesoscale or synoptic scale forcing associated with the precipitation process in LA clouds.

[17] Overall, the average BL segment durations are 50% greater than for LA clouds. This implies for the BL clouds less segment intermittency in terms of precipitation structure, as well as less mesoscale variability in general. We speculate that it also might indicate that mechanisms governing cloud system morphology are characterized by larger scales in BL cloud layers compared to LA cloud layers.

[18] Cloud system morphology for the four cloud system classifications may be more generally represented as PDFs of segment duration and is shown in Figure 2. We speculate that dissimilar mechanisms driving cloud formation and maintenance (e.g., surface fluxes, cloud top cooling, quasi-geostrophic ascent) within low cloud systems ultimately lead to differences in variability characteristics, represented by differences in segment length. Relative differences between the mean and median in Table 1 imply skewed distributions, and the PDFs in Figure 2 confirm this. Particularly noticeable from Table 1 is the greater frequency of the shortest segments in LA clouds, relative to the BL classification. PDFs for all BL and LA clouds in Figure 2c confirm the short-term intermittency of the LA cloud category, particularly for timescales under 30 minutes.

3. PDF-Based Characterization of Cloud System Variability

3.1. Statistics of the Two Moments of Reflectivity PDFs

[19] The variability of each cloud segment is described by a PDF of reflectivity and its first and second moments. The box plots in Figures 3 and 4 present comparative statistics related to the first and second moments of the reflectivity PDFs. The dot and the horizontal bar in the box is the distribution mean and median, respectively. The range occupied by the box (where the central 50% of the data are located) and the relative position of the mean and median shows the dispersion and skewness of the distribution, thus providing an indication of variety of PDF shapes.

[20] As expected, the width of the distribution first moments $\overline{Z}_i$ is largest for the complete, unstratified category (marked "All" in Figures 3a and 4a). Stratifying segments into precipitating and nonprecipitating categories decreases the width of the distribution of segment means $\overline{Z}_i$, particularly for the nonprecipitating segments. The scatter in $\overline{Z}_i$ also slightly decreases with scale, since resampling over successively larger subsegments effectively truncates any variability at scales smaller than the subsegment. For nonprecipitating segments of both types the distributions are almost symmetrical, while positively skewed for precipitating segments. The skewness of precipitating segments is more pronounced in the BL category and less for the LA clouds. LA segments tend to have larger means than their BL counterparts, likely the result of greater liquid water content and thicker clouds arising from stronger forcing. The scatter of $\overline{Z}$ is not directly related to the primary measure of variability characterized by the second moment σ, which is plotted in Figures 3b and 4b. Analysis of the second moment sets $\{\sigma_i\}$ shows significant differences in cloud system variability between the various classifications. The wide range of standard deviations, as illustrated by the width of the box and whiskers, shows a dramatic scatter in the width of the segment PDFs. As expected, LA clouds exhibit significantly more variability relative to BL clouds (e.g., $\langle\sigma\rangle$ for LAp 40% greater than $\langle\sigma\rangle$ for BLp). Here $\langle\ \rangle$ denotes averaging over all segments, for example $\langle\sigma\rangle = \sum_{i=1}^{nsegments} \sigma_i$. Drizzling clouds exhibit greater variability compared to nondrizzling counterparts (e.g., $\langle\sigma\rangle$ for LAp is 60% greater than $\langle\sigma\rangle$ for LAnp), with drizzling LA clouds exhibiting the greatest variability among all categories.

[21] Standard deviation σ increases significantly with scale: the 10 km subsegments have the smallest σ, followed by the 30 km subsegments, and finally, the original full-length segments. To explore in greater detail the increase in

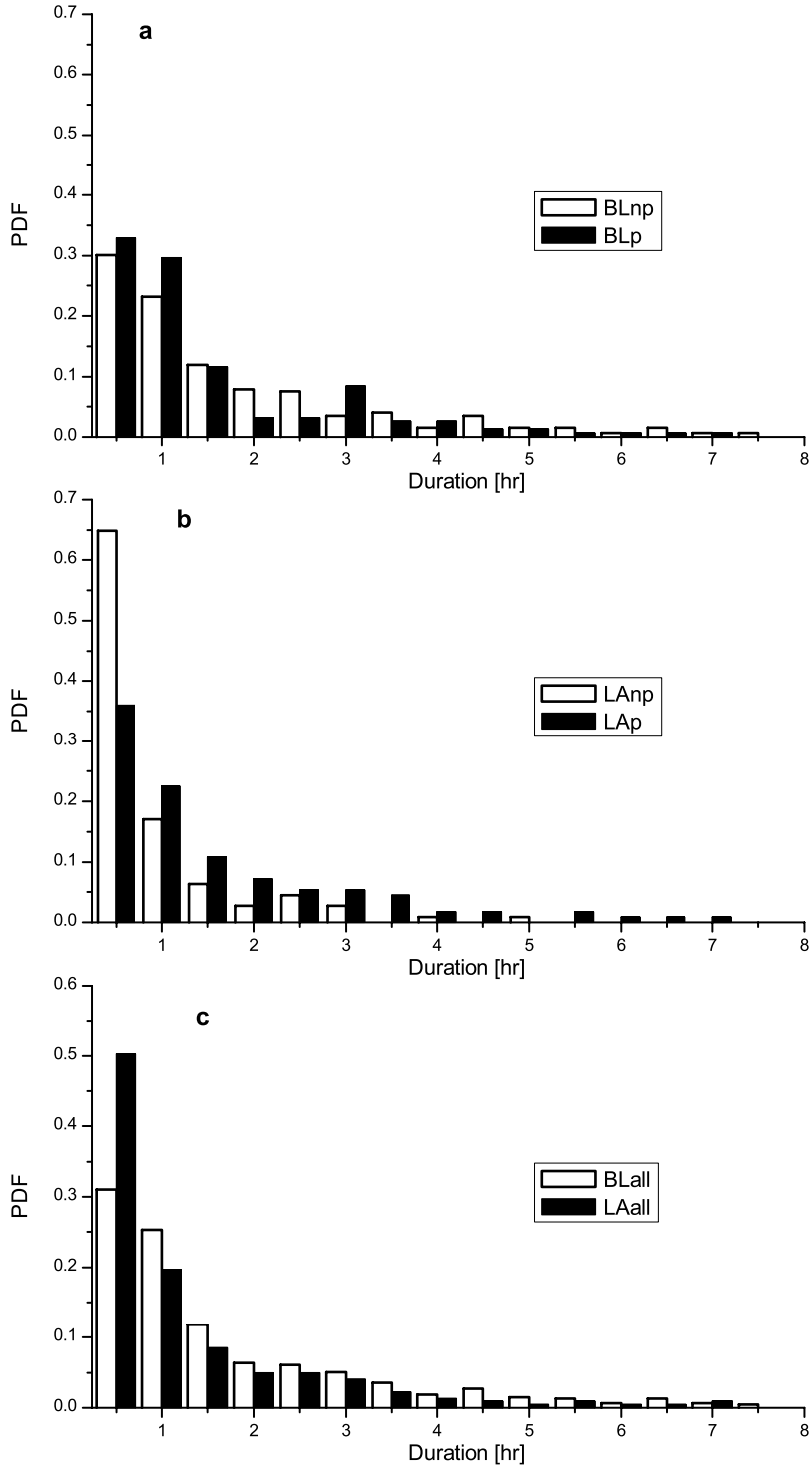

Figure 2. Frequency distribution of segment duration for nonprecipitating and precipitating (a) BL and (b) LA segments and (c) for all BL and LA cloud segments. Bin size is 0.5 hour.

σ with scale, we calculated PDFs for sets of $\{\sigma_i\}$ for different subsegment lengths. Figure 5 shows the PDFs plotted as a function of subsegment length by stacking the PDFs horizontally and contouring equal values of probability. Not surprisingly, the variability generally increases with scale. For example, in LA clouds the mean σ for 100 minute segments is more than double the mean for 5 minute segments. The greatest sensitivity to scale occurs at the smallest scales, less than 30 and 60 minutes for BL and LA clouds, respectively. This peak in sensitivity may be dictated by physical mechanisms that drive variability on these particular scales (18 and 36 km when translated to distance assuming a 10 m s^{-1} advection velocity). Examples of mechanisms that might drive mesoscale variability on scales smaller than about 40 km are gravity waves, shallow convective phenomenon, and nonlinear interactions related

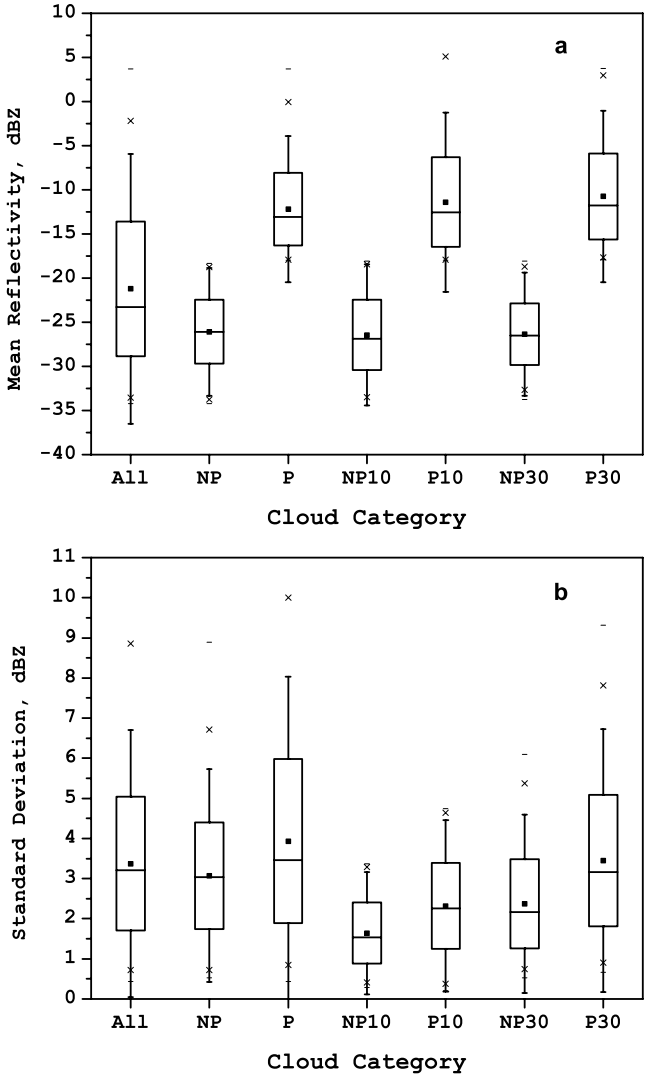

Figure 3. Box plots of first and second moments of reflectivity PDFs for each segment type in the BL category. (a) Mean. (b) Standard deviation. From left to right, boxes are all segments, nonprecipitating segments, precipitating segments, nonprecipitating 10 km subsegments, precipitating 10 km subsegments, nonprecipitating 30 km subsegments, and precipitating 30 km subsegments. The dot and the horizontal bar in the box are the distribution mean and median, respectively. The box top and bottom boundary represents the 25% and 75% (quartiles), the whiskers correspond to 5% and 95%, crosses correspond to 1% and 99% of the data, and minuses represent data minima and maxima.

to the emergence of organization in mesoscale convective cells. The larger-scale processes (e.g., 2-D eddies from horizontal wind shear instability, large-scale radiative forcing, quasi-geostrophic convergence/divergence) have a weaker effect on reflectivity variability.

[22] An important implication of the scale dependence of these statistics is that any treatment of subgrid variability in a cloud parameterization may depend on model grid size. The consequence of substantial scale sensitivity must be considered when comparing model results and observations, because of potential scale-related mismatches [*Liu et al.*, 2002; *Li et al.*, 2005].

3.2. Shape of Reflectivity PDFs

[23] To this point, variability has been characterized by the first and second moments of PDFs. However, the shape of the full PDFs, beyond simply the first two moments themselves, is described by higher-order moments as well and also provides important information on variability. Figure 6 illustrates large variety of PDF shapes by showing examples of seven PDFs selected from the data set of 150 BLnp segments. The top panel shows original PDFs, while the bottom panel displays the same PDFs, but centered on the corresponding mean value and shown as a function of reflectivity normalized by the standard deviation. Figure 6 illustrates the presence of single and double peaked, as well as symmetrical, positively, and negatively skewed PDFs.

[24] Another illustration of the scatter in PDFs shapes is given by Figure 7, where we present the average of all 150 PDFs in the BLnp category and its one and three standard deviation envelopes (the average PDF plus 1σ and 3σ). Figure 7 shows that the standard deviation of the PDF is of

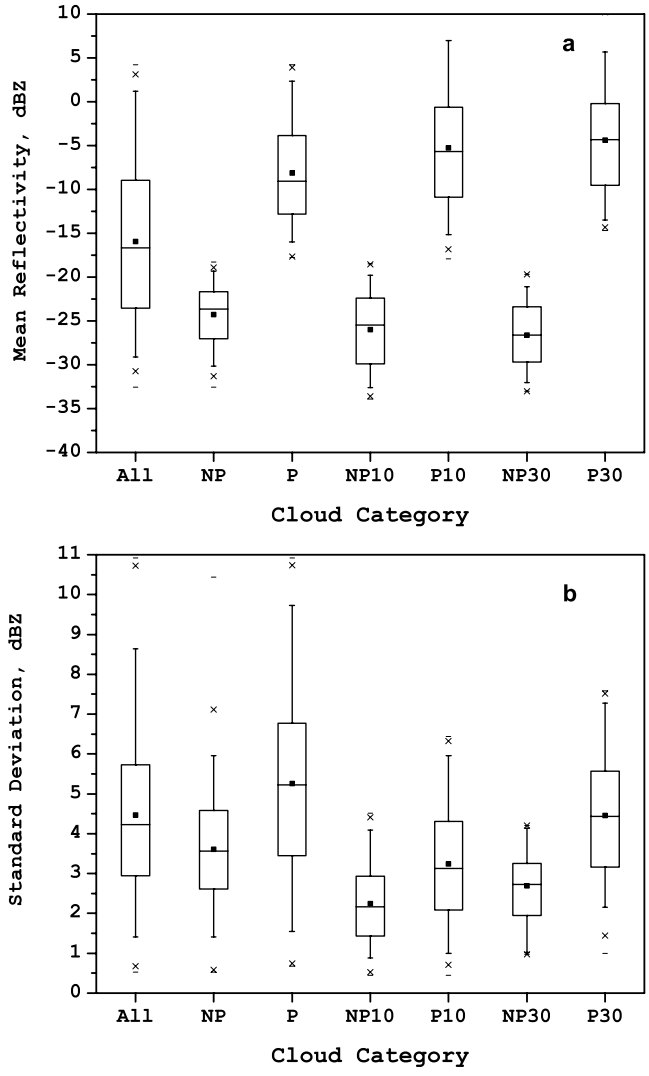

Figure 4. As in Figure 3 except for the LA cloud category.

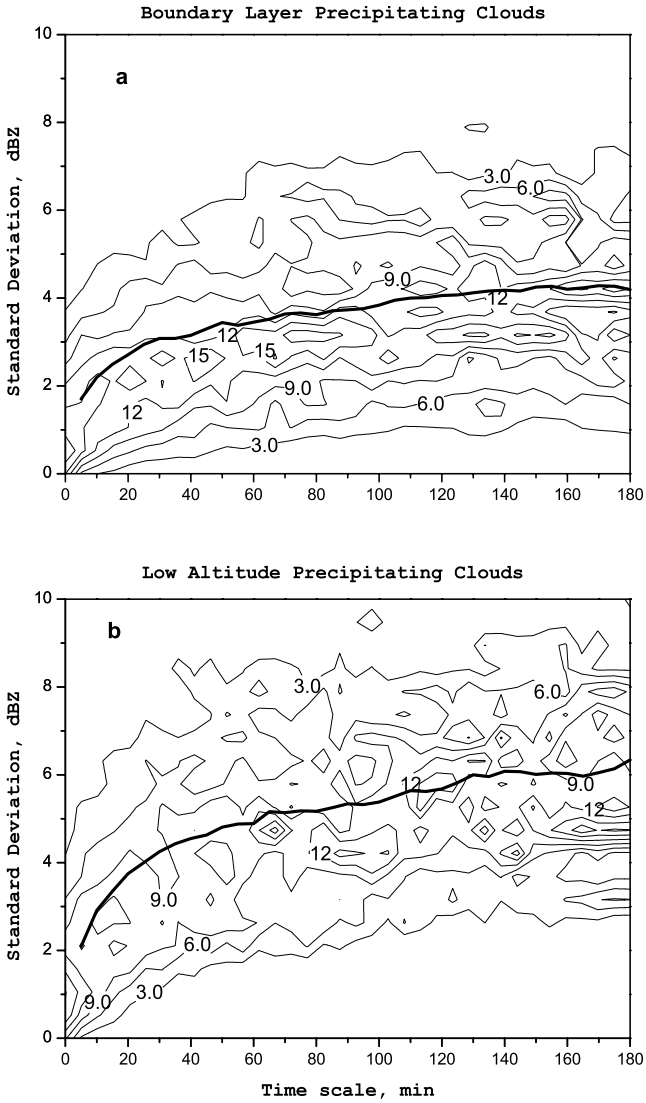

Figure 5. Isopleths (contour interval 3%) of probability distribution function for the standard deviation of reflectivity as a function of scale (subsegment length) for the data sets denoted in the plot panels. The thick solid line represents the mean standard deviation.

the same order as the average PDF itself. This conclusion is true for the BL, as well as LA clouds. It is clear that, despite the fact that stratifying low-layer clouds into categories by cloud type, the presence of precipitation, and scale substantially reduces the scatter of the moments, nevertheless, the scatter in PDFs remains quite large and assigning a single, unified PDF to each category may be a very crude, inadequate description of variability.

4. Characterization of Cloud Variability With Assumed PDFs

4.1. Empirical Relationship Between Second and First Moments

[25] The most straightforward way to define a PDF is to assume that it can be represented by a known analytical function, for example Gaussian or combination of Gaussian functions with a certain number of degrees of freedom [e.g., *Larson et al.*, 2001b]. We first consider a two-moment Gaussian distribution with the first moment representing the resolved model quantity and the second moment defined by some closure scheme. The simplest way is to assume a constant second moment [see, e.g., *Considine et al.*, 1997; *Lohmann et al.*, 1999], in effect reducing the degrees of freedom from two to one. Our results, however, show that for any single cloud category the second moment varies over a wide range, therefore using a fixed second moment is a rather crude approximation which most likely will produce a poor fit with the observed PDFs and inaccurate estimates of unbiased process rates. A better solution is to

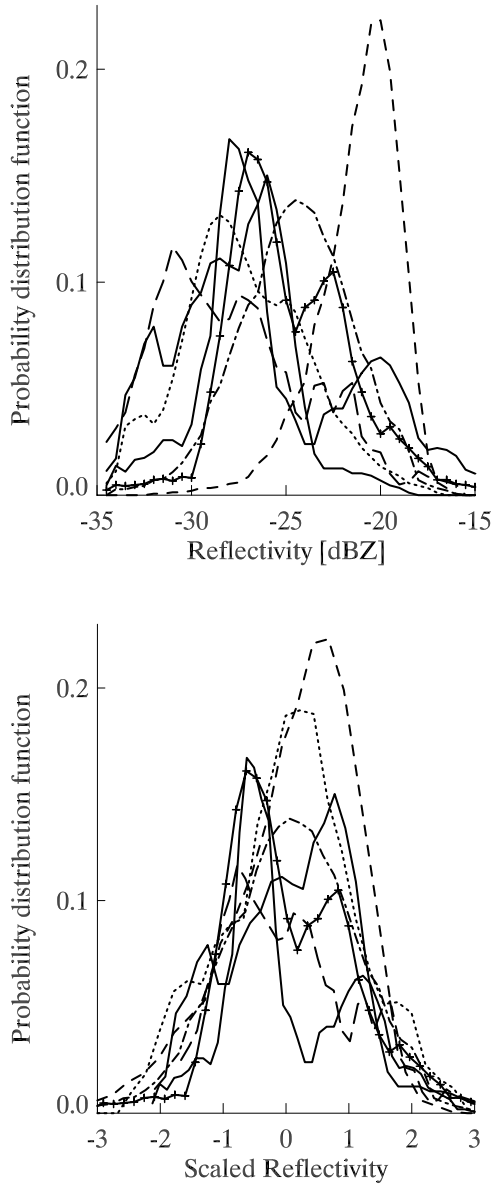

Figure 6. A sample of seven PDFs of reflectivity selected from the data set of 150 BLnp segments with duration more than 1 hour. (top) Original PDFs and (bottom) the same PDFs centered at their corresponding mean values and scaled by the standard deviation.

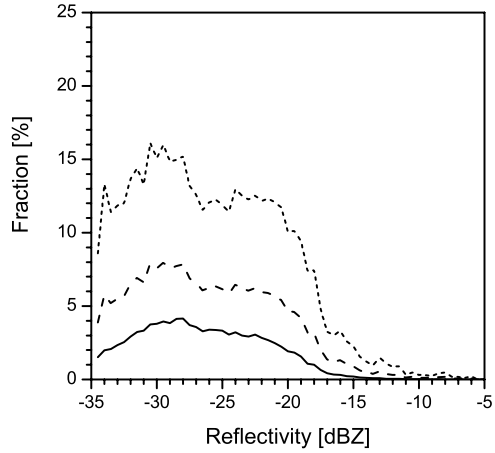

Figure 7. Mean of PDFs of reflectivity for 150 BLnp segments with duration more than 1 hour (solid line). Dashed lines represent mean plus 1σ and 3σ.

find a relationship between the second moment and first moments.

[26] We seek the functional dependence of the second moment to the first moment separately for each cloud type (BL and LA) and scale (10 and 30 km). Note that we do not stratify cloud segments by the presence of drizzle, since the explicit dependence of the variance on $\overline{Z}$ allows for both drizzling and nondrizzling segments. Data segments are binned according to their first moment (mean reflectivity) into 1 dBZ intervals (or 2 dBZ intervals, if the number of segments in the set is small) over the entire domain of reflectivity, and linear regression is applied to find the least squares fit $\sigma = f(\overline{Z})$ to the observational data.

[27] Figures 8 and 9 show the dependence of standard deviation on the mean for 30 km and 10 km BL and LA subsegments, respectively. The standard deviation is smoother in the vicinity of bins with a larger number of points, and only bins with 10 points or more are used in the calculation of the regression line. Figures 8 and 9 all demonstrate a systematic increase in σ with mean reflectivity. Although σ for BL clouds is significantly smaller than for LA clouds, the 30 km BL category shows the greatest sensitivity — a quadrupling over the entire range of reflectivity (Figure 8a). Variability in LA clouds, on the contrary, is greater in general, but not as sensitive to changes in mean reflectivity. As for BL clouds, in the LA category the larger scale size is associated with greater sensitivity, as shown by the steepness of the linear fit. Not only do these results indicate the expected result that larger scales are associated with greater variability, the increase of sensitivity with scale also suggests that assuming a constant σ becomes particularly detrimental as the scale size increases.

[28] The main result of Figures 8 and 9 is that the standard deviation may be determined as a function of mean reflectivity $\overline{Z}$ with an error on average of about 30–40%. Within the range of reflectivity where drizzle occurs ($Z > -17$ dBZ), the number of segments is fewer and the relationship is noisier, but nevertheless the parameterization $\sigma = f(\overline{Z})$ may be well represented by a linear function:

$$\sigma = \alpha + \beta\overline{Z} \qquad (1)$$

[29] Here the parameters α and β depend on grid size and cloud type. Table 2 shows these values for the BL and LA cases together with correlation coefficients for both grid sizes. Values of α represent the baseline variance and β expresses the sensitivity to mean reflectivity. The linear dependence (1) and the magnitude of the scatter are consistent with *Considine et al.* [1997], who presented a model that showed a linear relationship between standard deviation and mean for cloud liquid water path. Their model derived relationship was compared and found consistent with the LWP retrievals using Landsat data (B. A. Wielicki and L. Parker, unpublished data, 1994).

[30] Results summarized in Figures 8 and 9 reiterate the conclusions made in previous sections. Specifically, the standard deviation (1) strongly depends on cloud type and is greater for low-altitude clouds, (2) increases with scale, and (3) increases with reflectivity. The last point is consistent with the notion that drizzling clouds with larger

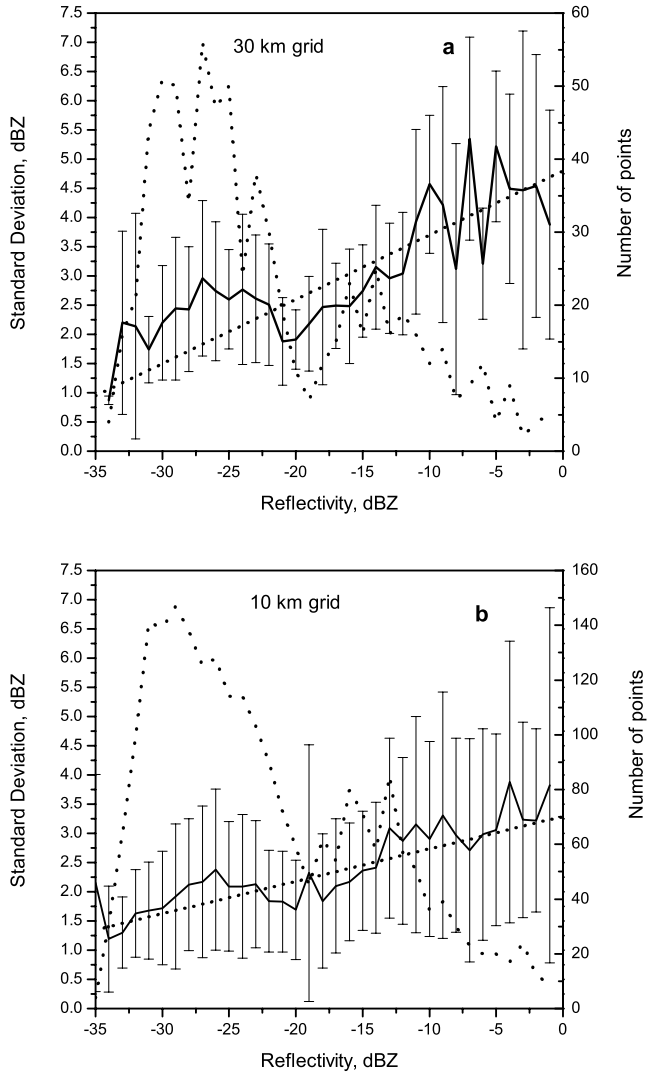

Figure 8. Standard deviation σ (thick solid line) with its standard deviation σ_σ denoted by error bars, as a function of mean reflectivity, for BL cloud segments. Dotted line represents number of samples per bin. (a) 30 km scale and 2 dBZ bin size. (b) 10 km scale and 1 dBZ bin size.

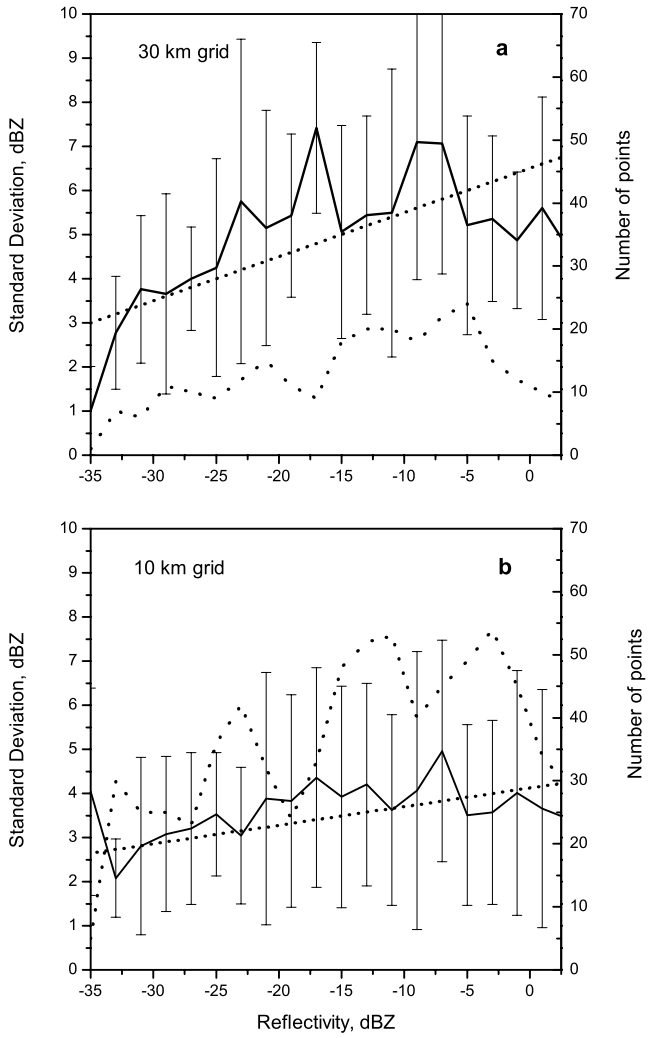

Figure 9. As in Figure 8 but for LA cloud segments. Both scales use a 2 dBZ bin size.

reflectivity exhibit greater variability relative to nondrizzling clouds. Furthermore, because reflectivity is proportional to the sixth power of the drop size distribution, the increase in variability with reflectivity suggests the importance of microphysical processes that control drop growth. However, our data do not preclude the possibility of the converse, namely that the physical processes that favor greater variability may also enhance drizzle production. What is clear is that drizzle and variability are interdependent.

4.2. Comparing Unbiased Subgrid Variability Quantities From Assumed and Observed PDFs

[31] Point observations and grid point quantities in numerical models have a characteristic scale (spatial, temporal, or both) associated with them. Fluctuations occurring between samples in an observational network constitute variability on scales finer than the sampling frequency or spatial scale, while numerical model grid point quantities typically represent the grid volume mean, but neglect variability on scales finer than the grid mesh (for finite difference formulations). Biases in process rates and other diagnostic grid mean quantities (e.g., albedo) can arise when ignoring subgrid variability. The bias tends to increase with grid size, as the subgrid distribution becomes wider and the additional variability is not represented by the model grid point quantities. Furthermore, *Pincus and Klein* [2000] showed that subgrid variability bias depends not only on the character of the variability, but also on the degree of nonlinearity in the process rate.

[32] As an illustration of the impact of subgrid variability on microphysical quantities, we applied PDFs of low cloud radar reflectivity and a *Z-R* relationship to calculate biases in precipitation flux that would arise by neglecting subgrid heterogeneity. We applied the following widely used form to calculate precipitation flux from radar reflectivity,

$$Z_r = aR^b \tag{2}$$

where R is precipitation rate [mm h^{-1}], Z_r is the radar reflectivity factor in mm^6 m^{-3} and may be expressed in logarithmic units as $Z = 10 \log_{10} (Z_r/1\ mm^6\ m^{-3})$ [dBZ]. The parameters a and b (25 and 1.3, respectively) are suggested by *Comstock et al.* [2004] on the basis of observations from field campaigns in different Sc regimes.

[33] The effect of unresolved variability is estimated by the bias, which is assessed by the ratio

$$B = \frac{\left[R(\overline{Z}) - \overline{R(Z)}_{true}\right]}{\overline{R(Z)}_{true}} \tag{3}$$

Here $\overline{R(Z)}_{\text{true}}$ is the unbiased precipitation flux calculated by integrating the *Z-R* relationship over the 'true' observationally derived PDF. $R(\overline{Z})$ is the precipitation flux calculated from the mean of the PDF and neglects subgrid variability. Since $\partial^2 R/\partial Z^2 > 0$, then $R(Z)$ is a convex function, and the errors arising from the neglect of subgrid variability will be consistently negative, always underestimating precipitation flux (see *Larson et al.* [2001a] for a more thorough mathematical foundation).

[34] The pluses in Figure 10 show subgrid variability bias (3) as a function of segment standard deviation for BL and LA clouds. As anticipated, for both categories the bias is strongly dependent on the variability of the segment, with larger segment standard deviations associated with larger bias. The maximum bias in both categories reaches ~70% for large standard deviations. The average bias is −26% and −35% for BL and LA clouds, respectively, so ignoring subgrid variability in this case would result in a significant underestimation of precipitation flux. The bias depends not only on the subgrid variance but also on the nonlinearity of the process rate, in particular, on the value of exponent b. For example, BL and LA average biases increase to 54% and 63%, respectively, when b is decreased from 1.3 to 0.7.

Table 2. Coefficients of the Standard Deviation Parameterization (Equation (1))

Cloud Type	Scale, km	α[dBZ]	β	*R*
BL	10	3.45	0.058	0.88
BL	30	4.61	0.093	0.83
LA	10	4.24	0.038	0.63
LA	30	6.30	0.069	0.60

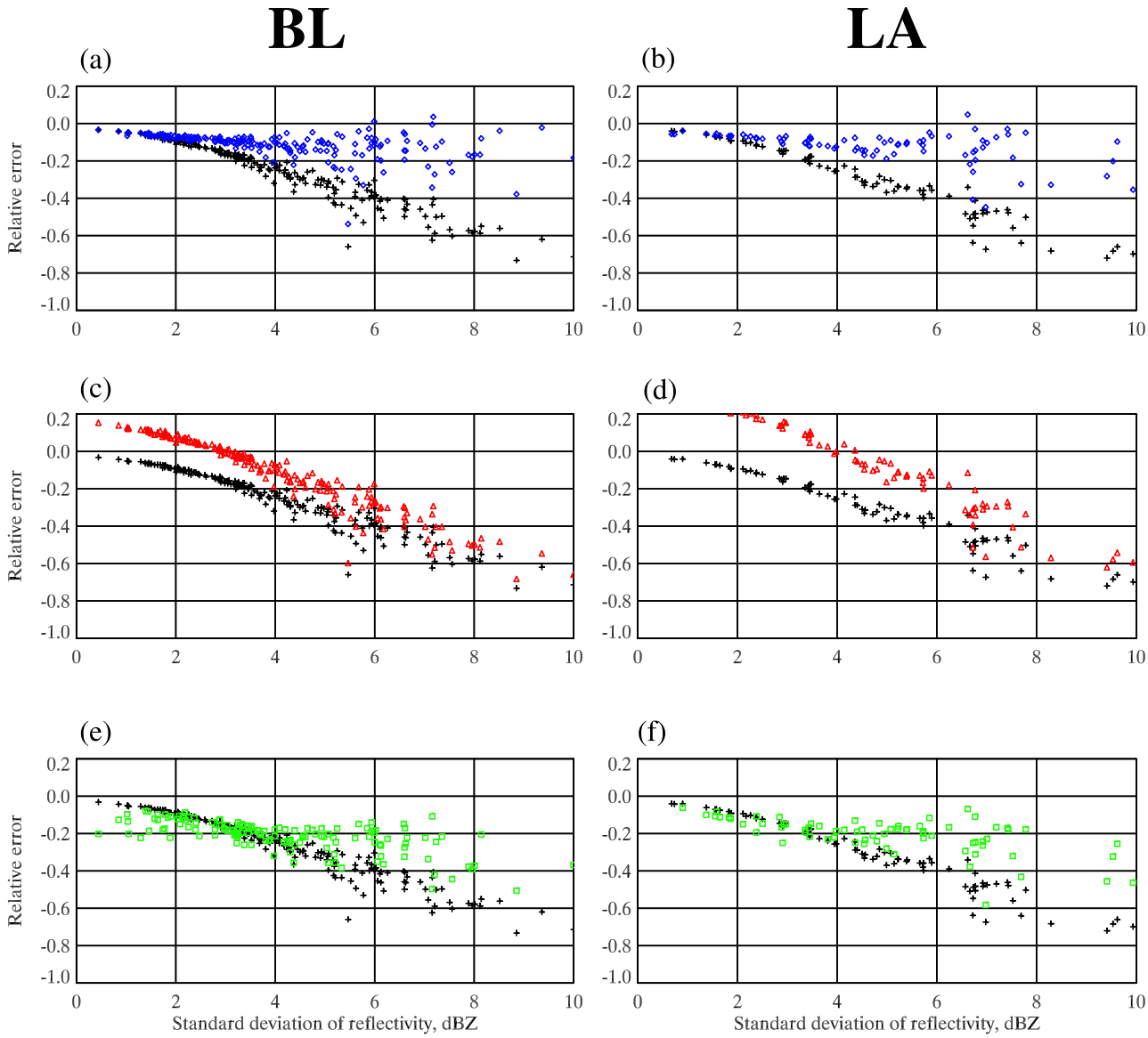

Figure 10. Relative error in grid volume mean precipitation flux, assuming three analytic approximations to the full PDF for all BL (left) and LA (right) cloud segments. Black pluses represent error from assuming zero variability, i.e., the subgrid variability bias. (a–b) Accounting for variability by 2*P* approximation with the mean and standard deviation taken from the observed PDF. (c–d) Accounting for variability by *FS* approximation, with the mean taken from the observed PDF and a standard deviation equal to the average standard deviation of all segments in each cloud category. (e–f) Accounting for variability by *GM* approximation, with parameters determined by the mean and standard deviation taken from the observed PDF.

[35] In numerical models, subgrid variability would most likely be approximated by an analytic PDF characterized by lower-order moments like mean and standard deviation. Figure 10 shows the relative errors of using three different analytic approximations to the observational MMCR PDFs: (1) 2*P*, a two-parameter Gaussian distribution with the mean and standard deviation equal to those of the observational PDF (blue diamonds); (2) *FS*, a fixed sigma Gaussian distribution with the mean equal to the observational PDF mean, but with the fixed standard deviation equal to the average of observational ('true') PDF standard deviations (red triangles); and (3) *GM*, a Gamma distribution with the mean and standard deviation equal to the corresponding observational PDF values (green squares).

[36] The relative errors of these analytical approximations is assessed by the ratio

$$Err = \frac{\left[\overline{R(Z)}_{aa} - \overline{R(Z)}_{true}\right]}{\overline{R(Z)}_{true}} \tag{4}$$

where $\overline{R(Z)}_{aa}$ is the precipitation flux calculated by integrating the *Z-R* relationship over the analytically

approximated (*aa*) PDF. A perfect fit between the analytic and observed PDFs would lie along the zero line.

[37] Among all analytical approximations shown in Figure 10, the best is given by the 2P approximation (blue diamonds in Figures 10a and 10b). The *Z-R* relationship is integrated over a truncated Gaussian distribution from −35 dBZ to the upper bound of the observed PDF. This truncation reduces contributions from the right hand tail of the analytic distribution that may in fact not be present in the observational PDF. On average, the 2*P* approximation accounts for about 75% of the subgrid variability bias for both cloud types, especially for low and moderate measures of variability (less than 5 dBZ). For segments with larger variability, the 2*P* approximation still represents a significant fraction of the error, though somewhat less, because of the deviation from symmetry of the observed PDFs. This result implies the possible importance of the third moment — skewness — which may need to be taken into account in order to more completely characterize cloud variability.

[38] Assuming a subgrid distribution with fixed standard deviation would be a natural first step above assuming horizontal homogeneity, but Figures 10c and 10d show that the performance of the *FS* approximation is less than satisfactory. The FS approximation overestimates the variability for segments of low standard deviation, leading to instances of positive error and overestimates of grid mean precipitation flux. For segments of larger variability, the variability and grid mean flux are underestimated. Only for the small number of cases where the segment standard deviation is nearly equal to the fixed value is the error near zero. Figures 10e and 10f show the error characteristics using the *GM* approximation. The error arising from the Gamma distribution approximation is, in general, between the 2*P* and *FS* approximations.

[39] The error calculations are also sensitive to the truncation method employed, since the nonlinearity of the *Z-R* relationship accentuates contributions in the right hand tail of the distribution. Not truncating the analytic PDFs can even lead to positive bias (overestimate) in grid mean quantities. The truncation used in the bias calculations in Figure 11 is based on the upper bound of each observational PDF and may be thought of as an additional degree of freedom. How should this constraint be implemented in a statistical scheme that uses analytical representations of subgrid variability? We tested two approaches which, along with the truncation method based on the upper bound of each PDF, are summarized in Table 3 as mean relative error induced by the approximation and truncation methods. The simplest approach of specifying a single truncation value representative of the mean of all observed PDFs performs very poorly relative to truncating each PDF individually on the basis of its upper bound. A statistically based approach of truncating the analytic PDF at $\overline{Z} + 2\sigma$ gives results comparable (if not better) than truncating the PDFs individually. Of the three approaches, this is the most logical to employ, since in any treatment of subgrid variability the variance σ will be either predicted or diagnosed and thus will be readily available.

[40] Figure 11 shows errors introduced by using the linear relationship (1) for the second moment in comparison with the errors introduced by the *FS* approximation with fixed value of standard deviation $\sigma(Err_\sigma)$. As the relationship (1) was obtained for the fixed 10 and 30 km scales, the two fixed scale subsets were extracted from the data shown in Figure 10 and used for error calculations presented in Figure 11. To assess the effect of the errors for the whole data set as opposite to the errors of individual data segments, we also show cumulative errors as a function of standard deviation in each subset:

$$E(\sigma) = \int_0^\sigma |Err(s)|ds \tag{5}$$

[41] Here $|Err(s)|$ is the absolute value of the bias calculated for each individual cloud segment with the standard deviation s according to (4). For display purpose, we normalize the cumulative errors by the maximum error in the linear closure case. The error of the *FS* approximation is very sensitive to the value of the standard deviation σ used to define the distribution. The three curves shown in Figure 11 correspond to the values of σ equal to σ_a, $\sigma_+ = \sigma_a + \delta\sigma_a$, and $\sigma_- = \sigma_a - \delta\sigma_a$, where σ_a is the average standard deviation of observational PDFs and $\delta\sigma_a$ is its standard deviation.

[42] The results of Figure 11 show the improvement given by the linear closure model compared to the *FS* approximation. The difference is most clearly seen in the plots of cumulative error curves (Figures 11c and 11d). The linear closure works best when σ is in the low to medium range of values. The performance of the *FS* approximation, on the other hand, is highly sensitive to the choice of the standard deviation. The latter is not known a priori, therefore when its guess is close to the average standard deviation of the data set, the *FS* approximation performs nearly as well as the linear closure model. However, the deviations from the average value result in a significant increase of errors, even in the small variability range.

[43] The performance of the symmetrical Gaussian approximation is better than one would expect given the wide range of PDF shapes exemplified by examples of PDFs shown in Figure 6. It demonstrates the principal role of the width parameter (standard deviation) in defining the PDF. Further improvements, especially in cases with large standard deviation, may necessitate the use of higher moments of the PDF, primarily the skewness parameter, which may be accounted for by using double Gaussian approximations [see *Larson et al.*, 2001b]. Our results thus imply that commonly employed analytical distribution functions are often reasonable approximations for radar reflectivity PDFs, particularly when care is taken in determining how to truncate the analytic PDFs prior to integration.

[44] We do not intend that our PDFs of reflectivity and calculations of grid mean precipitation rates be incorporated directly into statistical cloud schemes, which are currently cast in geophysical quantities characterizing liquid water content. Nevertheless, the results serve as a gauge of how well lower-order moments and assumed distributions (as opposed to the much more complicated and widely varying observational PDFs) are able to represent subgrid variability for the purpose of nonlinear grid mean processes.

[45] The presented in this section results illustrate the performance of various formulations of subgrid variability

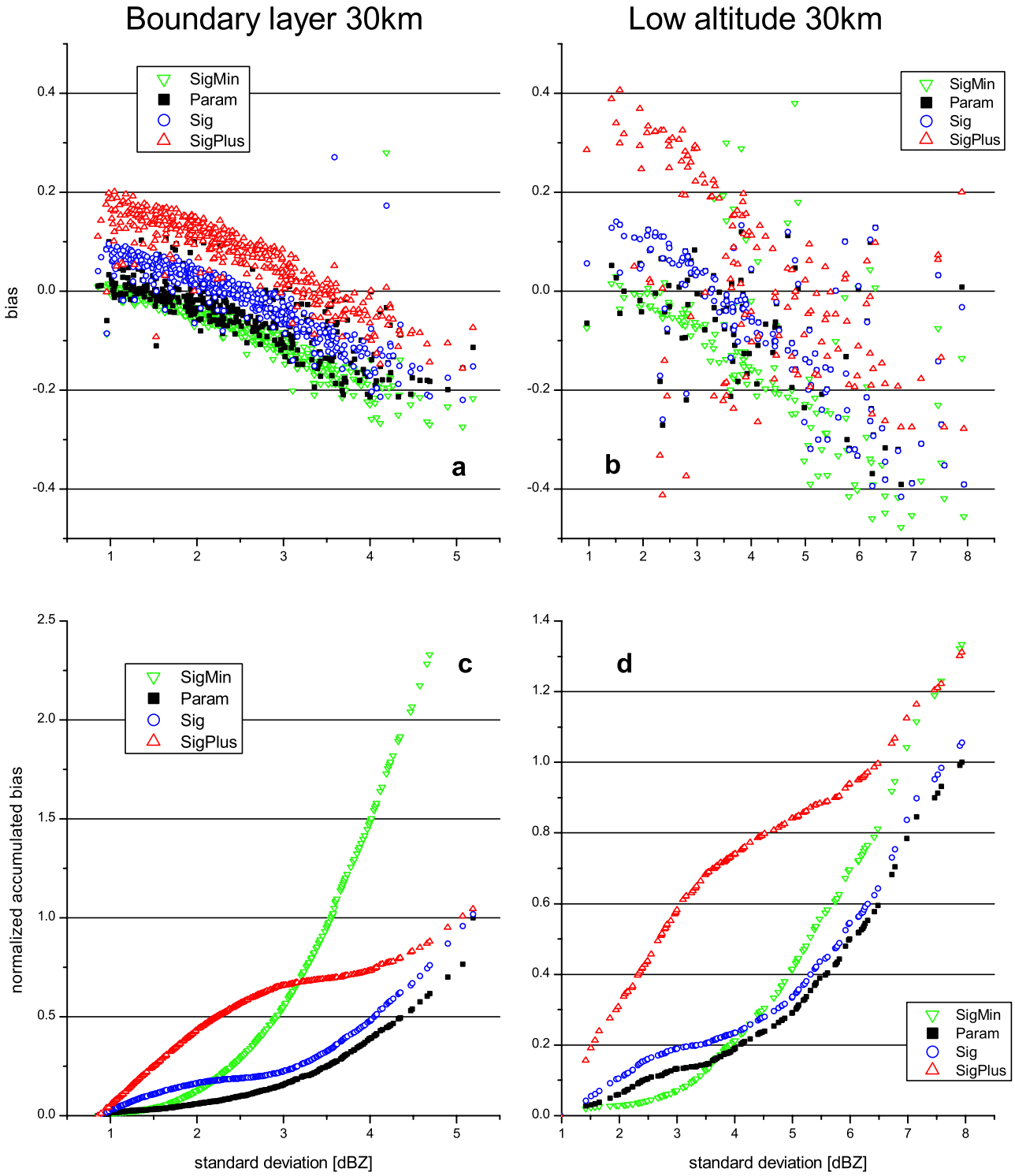

Figure 11. Scattergram of (a and b) point-by-point and (c and d) normalized accumulative bias versus standard deviation for 30 km cloud segments for 4 scenarios: (1) when variability is accounted by two-parameter Gaussian PDF with the second moment closure according to equation (1) (squares); (2) when variability is accounted for by *FS* approximation with the standard deviation σ equal to mean standard deviation (circles); and (3) and (4) with σ equal to σ_+ and σ_- (see text for detailed explanation).

Table 3. Mean Relative BL Precipitation Flux Errors Associated With Different PDF Truncation Methods for the Three Analytic PDF Approximations[a]

	2P Gaussian	FS Gaussian	Gamma
Individual PDF upper bounds	0.14 (0.16)	0.22 (0.28)	0.21 (0.24)
Mean of all PDF upper bounds	0.26 (0.33)	0.28 (0.41)	0.33 (0.37)
$\overline{Z} + 2\sigma$	0.11 (0.13)	0.20 (0.26)	0.19 (0.21)

[a]Errors for LA clouds are enclosed in parentheses.

in computing the precipitation flux. Similar analyses directly applicable to numerical models could be performed, for example using PDFs of liquid water content to assess unbiased grid mean autoconversion and accretion rates.

5. Summary and Conclusions

[46] The variability of unbroken, low-layer stratiform clouds over the ACRF SGP site is analyzed using more than 1000 hours of radar reflectivity observations over two winter seasons. Our study of cloud variability focuses on statistical characteristics of reflectivity probability distribution functions and the dependence of these parameters on cloud type, the presence of precipitation, and scale.

[47] We stratified radar observations of low cloud systems into stratocumulus cloud-topped boundary layer (BL) and low-altitude (LA) stratiform types. Cloud segments were also stratified by scale and the presence of precipitation. Nonprecipitating clouds tend to dominate the BL category, and about 85% of all observed BL clouds were either nonprecipitating or only lightly drizzling. In contrast, LA clouds over the ARM SGP site were less frequent and predominantly precipitating.

[48] Cloud system variability, as characterized by the standard deviation of the reflectivity σ, typically increases with the reflectivity. LA segments tend to have larger mean reflectivity than BL segments, and precipitating clouds are characterized by larger values of σ, particularly for the LA category. Variability is a strong function of scale and nearly doubles in the 20–100 min time scale range. The greatest scale sensitivity is present at small scales, from 5 to 30 min for BL clouds and from 5 to 60 min for LA clouds.

[49] Subgrid cloud variability in numerical models will most likely be described by lower-order moments of analytical PDFs. From the parameterization point of view, one crucial question is whether a single PDF may be applicable for all cloud types. Our results analyzing observational PDFs of radar reflectivity imply the negative — we believe that such a unified description is not possible. Our results, however, indicate that the uncertainty in the moments of the PDF may be substantially reduced if the cloud system is stratified by type and scale. In this case a probability distribution function based on two moments, the mean and the standard deviation, may be satisfactory for characterizing subgrid variability, especially for low-to-moderate variances.

[50] We apply the observational PDFs of reflectivity to estimate bias in precipitation flux arising from neglecting subgrid variability and suggest a general approach to the formulation of subgrid variability that employs a truncated Gaussian PDF. The use of a simple Gaussian type function is justified by our calculations, as long as the mean and the standard deviation are accurately represented. The Gaussian two-moment distribution is demonstrably more accurate than either the Gaussian with the fixed variance or the Gamma distribution. Further progress may necessitate the knowledge of the shape of PDF and use of higher moments of the PDF such as skewness.

[51] A relationship for the second moment is presented, based on the first moment and valid for fixed scales of 10 and 30 km, which are taken to be representative of mesoscale and NWP model horizontal grid sizes. Applying this relationship as a closure for the second moment results in a more robust estimate of grid mean precipitation fluxes, relative to assuming a fixed value of variance.

[52] These results primarily serve to show that lower-order moments and assumed probability distributions are able to represent adequately subgrid-scale inhomogeneity for the purpose of evaluating nonlinear grid mean processes rates. On a more basic level, the variability characteristics as laid out in PDFs and statistics of reflectivity can be compared with corresponding model-generated statistics to help validate numerical model cloud and microphysics parameterizations. We emphasize that although current numerical models do not include radar reflectivity as a prognostic variable, the methodology used in our analysis can be applied for analysis of data sets of other cloud parameters when such statistically significant large data sets become available in the future either from direct observations or obtained by sufficiently accurate retrieval methods.

Appendix A: Use of a Reflectivity Threshold for Discriminating Precipitating and Nonprecipitating Continental Low Clouds

[53] Use of reflectivity threshold for separating precipitating and nonprecipitating cloud is a common practice in analysis and microphysical retrieval of both marine and continental cloud systems, despite the uncertainties related to the choice of threshold value. Studies based on in situ aircraft drop spectra measurements for marine [*Frisch et al.*, 1995a, 1995b; *Baedi et al.*, 2002] and continental [*Baedi et al.*, 2002] clouds demonstrate the presence of a sharp, drizzle induced increase in reflectivity over the range from −20 to −15 dBZ, which strongly suggests the existence of a reflectivity threshold that separates drizzling and nondrizzling clouds. *Frisch et al.* [1995a, 1995b] indicate that radar reflectivity values lower than −18 dBZ are usually associated with nonprecipitating cloud layers, while reflectivities greater than −16 dBZ tend to be well correlated with the presence of droplets of diameter of 50 μm and greater, which we term drizzle. (The term drizzle in these studies, as well as here refers only to the presence in the cloud of drops with diameter larger than 50 μm. The precipitation on the surface or in the subcloud layer obviously cannot be uniquely determined using cloud reflectivity values alone.) *Baedi et al.* [2002] use drop spectra measurements for continental and marine stratiform clouds obtained during four field projects to show that clouds with reflectivities below a threshold of −20 dBZ are nonprecipitating. From in situ aircraft data, *Sauvageot and Omar* [1987] found a threshold of −15 dBZ for continental stratocumulus, and *Chin et al.* [2000] used this threshold for microphysical

Table A1. Sensitivity of Precipitation Partitioning to the Reflectivity Threshold[a]

Threshold, dBZ	BLnp Fraction and Relative Difference, %	LAp Fraction and Relative Difference, %
−20	0.615 (−11)	0.743 (6.1)
−19	0.632 (−5.6)	0.726 (3.7)
−18	0.676 (−2.0)	0.714 (2.0)
−17	0.690 (0.0)	0.700 (0.0)
−16	0.732 (6.1)	0.652 (−6.8)
−15	0.759 (10)	0.630 (−10)

[a]Relative difference (%) is shown in brackets.

retrieval of continental low stratiform clouds. Using drop spectra measurements, *Wang and Geerts* [2003] further demonstrated that in marine clouds the threshold is a function of height and varies between −19 and −16 dBZ within the middle third portion of the cloud layer. Similar findings were obtained by *Mace and Sassen* [2000]. They empirically determined for continental clouds observed over the ARM SGP ACRF that layers with maximum reflectivity significantly greater than −20 dBZ nearly always contain drizzle. This threshold was used by *Kato et al.* [2001] to identify nondrizzling clouds observed over the same site for microphysical retrievals.

[54] In this study we have chosen to use −17 dBZ as a threshold value. A threshold of −20 dBZ makes more sense in microphysical retrievals, since the presence of any precipitation whatsoever can corrupt the retrieval, and this threshold provides much higher probability that there would be no precipitating clouds in the retrieving sample. However, such a small reflectivity threshold may incorrectly classify a cloud segment as precipitating. Being free of the requirements of retrievals enables us to choose −17 dBZ as a threshold value. As such, some ''crosstalk'' (incorrectly classified cloud segments) between precipitating and nonprecipitating categories can be expected. Table A1 illustrates the sensitivity to reflectivity threshold of the partitioning between precipitating and nonprecipitating cloud segments for the two prevailing (highest fraction) classifications. Using a threshold of −17 dBZ, the partitioning fraction was 0.690 for BLnp and 0.70 for LAp segments. Changes in cloud category partitioning fraction relative to the fraction at the threshold value of −17 dBZ, used in this study, illustrate sensitivity to the reflectivity threshold. As the data from Table A1 show, varying the threshold between −20 and −15 dBZ results in relative changes to the category partitioning fraction of less than approximately ±10%.

[55] As an independent assessment of the fidelity of the −17 dBZ threshold value, we have classified a 2-month subset of the data set (127 cloud segments) by identifying the correlation between radar echo base (defined as the height where reflectivity exceeds −50 dBZ) and multisensor cloud base best estimate. Specifically, segments in which the radar echo extends below cloud base are classified as precipitating. The assessment by this independent method shows that in all segments classified as precipitating the reflectivity exceeds the −17 dBZ threshold and thus conservatively identifies drizzling segments (just as a −20 dBZ threshold in other studies robustly identifies nonprecipitating segments). However, the identification of nonprecipitating segments by this threshold method was less accurate. Error arises from incorrectly categorizing precipitating regions as nonprecipitating and is 4% for cloud segments that were unambiguously liquid phase. An additional error of 9% is due to a number of segments characterized by low reflectivity (less than −20 dBZ) that were obviously precipitating. These precipitating segments with anomalously low reflectivity were generally associated with in-cloud temperatures in the −7°C to −10°C range, which suggests the presence of predominantly ice phase particles. This independent method of categorizing precipitating and nonprecipitating cloud segments is itself not foolproof and is critically dependent on the cloud base estimate, which frequently tends to be a noisy signal. Even so, applying the method to a one month subset of the seven month data set illustrates that a reflectivity threshold of −17 dBZ is a reasonable choice in stratifying precipitating and nonprecipitating continental low cloud.

[56] **Acknowledgments.** The authors are grateful to anonymous reviewers for many constructive comments. This research was supported by the Environmental Sciences Division of the U. S. Department of Energy (through Battelle PNR contract 144880-A-Q1 to the Cooperative Institute for Mesoscale Meteorological Studies) as part of the Atmospheric Radiation Measurement Program and the ONR grants N00014-96-1-0687 and N00014-03-1-0304. Data were obtained from the Atmospheric Radiation Measurement (ARM) Program sponsored by the U.S. Department of Energy, Office of Science, Office of Biological and Environmental Research, Environmental Sciences Division.

References

Ackerman, T. P., and G. M. Stokes (2003), The Atmospheric Radiation Measurement program, *Phys. Today*, *56*, 38–45.

Baedi, R., R. Boers, and H. Russchenberg (2002), Detection of boundary layer water clouds by spaceborne cloud radar, *J. Atmos. Oceanic Technol.*, *19*, 1915–1927.

Belotchitski, A. (2002), Parameterization of cloud physics processes in marine stratocumulus based on integral moments of the drop spectra, M.S. thesis, 76 pp., Univ. of Okla., Norman.

Cahalan, R. F., W. Ridgway, W. J. Wiscombe, T. L. Bell, and J. B. Snider (1994), The albedo of fractal stratocumulus, *J. Atmos. Sci.*, *51*, 2434–2460.

Chin, H.-N. S., D. J. Rodriguez, R. T. Cederval, C. C. Chuang, A. S. Grossman, and J. J. Yio (2000), A microphysical retrieval scheme for continental low-level stratiform clouds: Impacts of subadiabatic character on microphysical properties and radiation budgets, *Mon. Weather Rev.*, *128*, 2511–2527.

Clothiaux, E. E., T. P. Ackerman, G. G. Mace, K. P. Moran, R. T. Marchand, M. A. Miller, and B. E. Martner (2000), Objective determination of cloud heights and radar reflectivities using a combination of active remote sensors at the ARM CART sites, *J. Appl. Meteorol.*, *39*, 645–665.

Comstock, K. K., R. Wood, S. E. Yuter, and C. S. Bretherton (2004), Reflectivity and rain rate in and below drizzling stratocumulus, *Q. J. R. Meteorol. Soc.*, *130*, 2891–2918.

Considine, G., J. A. Curry, and B. Wielicki (1997), Modeling cloud fraction and horizontal variability in marine boundary layer clouds, *J. Geophys. Res.*, *102*(D12), 13,517–13,525.

Curry, J. A., et al. (2000), FIRE Arctic Clouds Experiment, *Bull. Am. Meteorol. Soc.*, *81*, 5–30.

Del Genio, A. D., M.-S. Yai, W. Kovari, and K. K.-W. Lo (1996), A prognostic cloud water parameterization for global climate models, *J. Clim.*, *9*, 207–304.

Frisch, A. S., D. H. Lenschow, C. W. Fairall, W. H. Schubert, and J. S. Gibson (1995a), Doppler radar measurements of turbulence in marine stratiform cloud during ASTEX, *J. Atmos. Sci.*, *52*, 2800–2808.

Frisch, A. S., C. W. Fairall, and J. B. Snider (1995b), Measurements of stratus cloud and drizzle parameters in ASTEX with K_a-band Doppler radar and microwave radiometer, *J. Atmos. Sci.*, *52*, 2788–2799.

Golaz, J.-C., V. E. Larson, and W. R. Cotton (2002), A PDF-based model for boundary layer clouds. Part I: Method and model description, *J. Atmos. Sci.*, *59*, 3540–3551.

Hartman, D., M. Ockert-Bell, and M. Michelsen (1992), The effect of cloud type on Earth's energy balance: Global analysis, *J. Clim.*, *5*, 1281–1304.

Kato, S., G. G. Mace, E. E. Clothiaux, G. C. Liljegren, and R. T. Austin (2001), Doppler cloud radar derived drop size distributions in liquid water stratus clouds, *J. Atmos. Sci.*, *58*, 2895–2911.

Kim, B.-G., S. Klein, and J. Norris (2005), Continental liquid-water cloud variability and its parameterization using Atmospheric Radiation Measurement data, *J. Geophys. Res.*, *110*, D15S08, doi:10.1029/2004JD005122.

Klein, S. A., R. Pincus, C. Hannay, and K.-M. Xu (2005), How might a statistical cloud scheme be coupled to a mass-flux convection scheme?, *J. Geophys. Res.*, *110*, D15S06, doi:10.1029/2004JD005017.

Larson, V. E., R. Wood, P. R. Field, J. Golaz, T. H. Vonder Haar, and W. R. Cotton (2001a), Systematic biases in the microphysics and thermodynamics of numerical models that ignore subgrid-scale variability, *J. Atmos. Sci.*, *58*, 1117–1128.

Larson, V. E., R. Wood, P. R. Field, J. Golaz, T. H. Vonder Haar, and W. R. Cotton (2001b), Small-scale and mesoscale variability of scalars in cloudy boundary layers: One-dimensional probability density functions, *J. Atmos. Sci.*, *58*, 1978–1994.

Larson, V. E., J. Golaz, and W. R. Cotton (2002), Small-scale and mesoscale variability of scalars in cloudy boundary layers: Joint probability density functions, *J. Atmos. Sci.*, *59*, 3519–3539.

Li, Z., M. C. Cribb, F. Chang, A. Trishchenko, and Y. Luo (2005), Natural variability and sampling errors in solar radiation measurements for model validation over the Atmospheric Radiation Measurement Southern Great Plains region, *J. Geophys. Res.*, *110*, D15S19, doi:10.1029/2004JD005028.

Liu, Y., P. H. Daum, and J. Hallett (2002), A generalized system theory for the effect of varying fluctuations on cloud droplet size distributions, *J. Atmos. Sci.*, *59*, 2279–2290.

Lohmann, U. N., L. McFarlane, L. L. Levkov, K. Abdella, and F. Albers (1999), Comparing different cloud schemes of a single column model by using mesoscale forcing and nudging technique, *J. Clim.*, *12*, 438–461.

Mace, G. G., and K. Sassen (2000), A constrained algorism for retrieval of stratocumulus cloud properties using solar radiation, microwave radiometer, and millimeter cloud radar data, *J. Geophys. Res.*, *105*, 29,099–29,108.

Mellor, G. L. (1977), The Gaussian cloud model relations, *J. Atmos. Sci.*, *34*, 356–358.

Moran, K. P., B. E. Martner, M. J. Post, R. A. Kropfli, D. C. Welsh, and K. B. Widener (1998), An unattended cloud-profiling radar for use in climate research, *Bull. Am. Meteorol. Soc.*, *79*, 443–455.

Norris, J. R., and S. A. Klein (2000), Low cloud type over the ocean from surface observations. part III: Relationship to vertical motion and the regional surface synoptic environment, *J. Clim.*, *13*, 245–256.

Oreopoulos, L., and R. Davies (1998), Plane parallel albedo biases from satellite observations. part 1: Dependence on resolution and other factors, *J. Clim.*, *11*, 919–932.

Pincus, R., and S. A. Klein (2000), Unresolved spatial variability and microphysical process rates in large-scale models, *J. Geophys. Res.*, *105*, 27,059–27,065.

Price, J. D. (2001), A study on probability distributions of boundary layer humidity and associated errors in parameterized cloud fruction, *Q. J. R. Meteorol. Soc.*, *127*, 739–758.

Price, J. D., and R. Wood (2002), Comparison of probability density functions for total specific humidity and saturation deficit humidity, and consequences for cloud parameterization, *Q. J. R. Meteorol. Soc.*, *128*, 2059–2072.

Rotstayn, L. D. (2000), On the "tuning" of autoconversion parameterizations in climate models, *J. Geophys. Res.*, *105*, 15,495–15,507.

Sauvageot, H., and J. Omar (1987), Radar reflectivity of cumulus clouds, *J. Atmos. Oceanic Technol.*, *4*, 264–272.

Sommeria, G., and J. W. Deardorff (1977), Subgrid-scale condensation in models of non-precipitating clouds, *J. Atmos. Sci.*, *34*, 344–345.

Stevens, B., W. R. Cotton, G. Feingold, and C.-H. Moeng (1998), Large-eddy simulations of strongly precipitating, shallow, stratocumulus-topped boundary layers, *J. Atmos. Sci.*, *55*, 3616–3638.

Tompkins, A. M. (2002), A prognostic parameterization for the subgrid-scale variability of water vapor and clouds in large-scale models and its use to diagnose cloud cover, *J. Atmos. Sci.*, *59*, 1917–1942.

Wang, J., and B. Geerts (2003), Identifying drizzle within marine stratus with W-band radar reflectivity, *Atmos. Res.*, *69*, 1–27.

Wood, R., P. R. Field, and W. R. Cotton (2002), Autoconversion rate bias in stratiform boundary layer cloud parameterizations, *Atmos. Res.*, *65*, 109–128.

Y. L. Kogan, Z. N. Kogan, and D. B. Mechem, Cooperative Institute for Mesoscale Meteorological Studies, University of Oklahoma, 100 E. Boyd, Energy Center, Room 1110, Norman, OK 73019, USA. (zkogan@ou.edu)